AIP | Review of Scientific Instruments

Design and initial characterization of a compact, ultra high vacuum compatible, low frequency, tilt accelerometer

A. O'Toole, F. E. Peña Arellano, A. V. Rodionov, M. Shaner, E. Sobacchi, V. Dergachev, R. DeSalvo, M. Asadoor, A. Bhawal, P. Gong, C. Kim, A. Lottarini, Y. Minenkov, and C. Murphy

Citation: Review of Scientific Instruments **85**, 075003 (2014); doi: 10.1063/1.4890285
View online: http://dx.doi.org/10.1063/1.4890285
View Table of Contents: http://scitation.aip.org/content/aip/journal/rsi/85/7?ver=pdfcov
Published by the AIP Publishing

Design and initial characterization of a compact, ultra high vacuum compatible, low frequency, tilt accelerometer

A. O'Toole,[1,a),b)] F. E. Peña Arellano,[2] A. V. Rodionov,[3,c)] M. Shaner,[4,d)] E. Sobacchi,[5] V. Dergachev,[6] R. DeSalvo,[6,a),e)] M. Asadoor,[7,f)] A. Bhawal,[8,g)] P. Gong,[9,h)] C. Kim,[10] A. Lottarini,[11,i)] Y. Minenkov,[12] and C. Murphy[13]

[1]*Department of Mechanical and Aerospace Engineering, University of California, Los Angeles, 405 Hilgard Ave, Los Angeles, California 90095, USA*
[2]*National Astronomical Observatory of Japan, 2-21-1 Osawa, Mitaka, Tokyo 181-8588, Japan*
[3]*California Institute of Technology, Pasadena, California 91125, USA*
[4]*Mayfield Senior School, 500 Bellefontaine Street Pasadena, California 91105, USA*
[5]*Scuola Normale Superiore, Piazza dei Cavalieri 7, 56126 Pisa, Italy*
[6]*LIGO Laboratory, California Institute of Technology, MS 100-36, Pasadena, California 91125, USA*
[7]*Mayfield Senior School, 500 Bellefontaine Street Pasadena, California 91105, USA*
[8]*Arcadia High School, 180 Campus Drive, Arcadia, California 91007, USA*
[9]*Department of Precision Instrument, Tsinghua University, Beijing 100084, China*
[10]*California Institute of Technology, Pasadena, California 91125, USA*
[11]*Department of Computer Science, University of Pisa, Largo B. Pontecorvo 3, 56127 Pisa, Italy*
[12]*Sezione INFN Tor Vergata, via della Ricerca Scientfica 1, 00133 Roma, Italy*
[13]*School of Physics, The University of Western Australia, 35 Stirling Highway, Crawley, Perth, Western Australia 6009*

(Received 30 April 2014; accepted 2 July 2014; published online 23 July 2014)

A compact tilt accelerometer with high sensitivity at low frequency was designed to provide low frequency corrections for the feedback signal of the Advanced Laser Interferometer Gravitational Wave Observatory active seismic attenuation system. It has been developed using a Tungsten Carbide ceramic knife-edge hinge designed to avoid the mechanical 1/f noise believed to be intrinsic in poly-crystalline metallic flexures. Design and construction details are presented; prototype data acquisition and control limitations are discussed. The instrument's characterization reported here shows that the hinge is compatible with being metal-hysteresis-free, and therefore also free of the 1/f noise generated by the dislocation Self-Organized Criticality in the metal. A tiltmeter of this kind will be effective to separate the ground tilt component from the signal of horizontal low frequency seismometers, and to correct the ill effects of microseismic tilt in advanced seismic attenuation systems. © *2014 AIP Publishing LLC*. [http://dx.doi.org/10.1063/1.4890285]

INTRODUCTION

A compact, ultra high vacuum compatible tilt accelerometer has been developed to satisfy the very stringent sensitivity requirements at low frequency of Gravitational Wave detectors[1] and for use in rotational seismology.[2]

Precision tilt accelerometers are necessary because horizontal accelerometers and seismometers are strongly sensitive to tilt seismic noise through the coupling to Earth's gravitational acceleration field. Accelerometers are spring-mass systems from which the acceleration signal is extracted by measuring the suspended mass position with respect to the case. Because of the presence of Earth's gravitational acceleration g, a static tilt is detected as acceleration applied for an infinitely long time. This coupling is inevitable, due to the principle of equivalence, and at low frequency any ground tilt noise overwhelms the true horizontal acceleration signal. To subtract and eliminate the systematic error introduced by tilt noise in accelerometer signals, it is necessary to measure tilt with corresponding accuracy. Seismometers used to generate feedback signals for seismic isolation systems help to reduce linear seismic noise at high frequency, at the price of injecting low frequency tilt noise in the form of excess linear acceleration. Because of the lack of a tilt accelerometer satisfying the requirements formulated by Lantz in Ref. 1, the Advanced LIGO seismic attenuation was found to amplify the low frequency seismic motion by a factor of 100.[3] That motion can make the lock acquisition of Advanced LIGO's high finesse Fabry-Perot cavities difficult. A low finesse interferometer, operating at half the wavelength of the main one (green light), was introduced in Advanced LIGO to

a)Authors to whom correspondence should be addressed. Electronic addresses: amandajotoole@gmail.com and riccardo.desalvo@gmail.com
b)Present address: Michigan Technological University, 1400 Townsend Dr, Houghton, Michigan 49931, USA.
c)Present address: Department of Electrical Engineering, University of California, Riverside, California 92521, USA.
d)Present address: University of Edinburgh, Edinburgh, EH9 3JZ, United Kingdom.
e)Present address: University of Sannio, C.so Garibaldi 107, Benevento 82100, Italy.
f)Present address: Oklahoma State University, 219 Student Union, Stillwater, Oklahoma 74074, USA.
g)Present address: Carnegie Mellon University, 5000 Forbes Ave Pittsburgh, Pennsylvania 15213, USA.
h)Present address: School of Industrial and System Engineering, Georgia Institute of Technology, Atlanta, Georgia 30332-0205, USA.
i)Present address: Department of Computer Science, Columbia University, 1214 Amsterdam Avenue, New York, New York 10027, USA.

mitigate this problem and ease interferometer lock acquisition in presence of the excess of mirrors residual motion injected at low frequency by the feedback loops.[4,5] Even if the green-light interferometer allows easy lock acquisition, high precision tilt accelerometers satisfying Lantz's requirements would effectively diminish the amplitude of the low frequency movements of the higher suspensions stages, thus reducing the corrective forces required from the mirror suspension to maintain the mirror in its lock position. This is particularly useful in stormy weather times. Reduced residual motion in the upper stages will mitigate any possible mechanical or electrical noise up-conversions in the mirror suspensions. Up-conversion processes are suspected of having leaked noise into the Gravitational Wave signal bandwidth, and limited the performance of Virgo+.

A mechanical tilt accelerometer is a rotational pendulum made of a rigid beam suspended on a hinge from its center of mass; Giazotto provides a useful discussion of the operation of tilt accelerometers in Ref. 6. The tilt signal is extracted by measuring the beam angle with respect to the instrument's case. If suspended exactly from the center of mass, tilt accelerometers are intrinsically insensitive to linear acceleration, but also to static tilt. They are therefore ideal to subtract the tilt systematic errors from accelerometers. Sensitivity to horizontal acceleration is introduced by the fact that the bar must be hinged slightly above its center of mass to keep it from rotational instability. The offset of the hinge point from the center of mass also restores sensitivity to static tilt to the tilt accelerometer. For this reason tilt accelerometers are also known as tiltmeters, the two terms will be used almost equivalently in the rest of the paper. The cross-sensitivity to tilt of a horizontal accelerometer is large; being equal to θ g = 9.8 θ m/s^2 where θ is the tilt angle. The sensitivity of tilt accelerometers to linear acceleration can be less than one part in a thousand if the tilt resonance is tuned at low frequency. The residual sensitivity to linear acceleration is easily diagonalized off when pairing a tiltmeter with a horizontal accelerometer.

The rotational information of a tiltmeter can be either extracted in free arm or in feedback mode operation. In the first case, there is no feedback on the arm movement, some damping is applied to keep the seismic activity from exciting very large oscillation, and the position of the arm is simply recorded. The transfer function from the electrical signal to rotational acceleration can be complicated, and the sensitivity decreases as the second power of the frequency below the mechanical resonance.

In feedback mode, the angular position of the arm is kept fixed to its nominal working point, with a pure-torque actuator. The angular acceleration is equal to the applied feedback torque divided by the arm's momentum of inertia "I," with a small correction due to the residual motion of the arm.

The tilt accelerometer discussed here was designed for feedback operation, with LVDT (Linear Variable Differential Transformer) angular position readout and electromagnetic actuation. An interferometric readout was prototyped as well. It demonstrated good readout sensitivity but also identified technical difficulties that prevented its implementation at this time.

Limitations of elastic-hinge tilt accelerometers

It is possible to suspend the beam exactly from its center of mass and make the instrument nominally insensitive to linear acceleration by using the restoring torque of an elastic hinge to avoid rotational instability. In this case, the tilt accelerometer null signal indicates the elastic equilibrium point of the flexure, and not the actual tilt with respect to Earth's gravitational field direction. Therefore, when introducing an elastic angular restoring torque, any hysteresis of the spring produces a fake (constant) tilt acceleration signal. The hysteresis value may change after any tilt transient. Because hysteresis is only approximately a linear function of the past transients and cannot be predicted, random noise is injected. In addition any spontaneous fluctuation of the spring's equilibrium point cannot be distinguished from fluctuating tilt acceleration.

Metal flexure tiltmeters have been built using the softest available flexures to dilute, as much as possible, the mechanical noise of the metal. Not surprisingly it was observed that all metal flexure tiltmeters were ultimately overwhelmed by 1/f noise at low frequency. It is now understood that 1/f mechanical noise originates from collective dislocation activity (avalanches)[7] in the metal flexures. This elasticity noise is controlled by entanglement-disentanglement of dislocation behaving according to Per Bak's self-organized criticality theory.[8,9] The dislocation activity is energized by tilt motion itself, as well as other vibrations, thermal changes, internal thermal fluctuations, and other perturbations. Because of the previously unrecognized 1/f noise of the flexure, high tilt sensitivity could be achieved only at relatively high-frequency.[10,11] The flexure 1/f noise can be mitigated, but not eliminated, by dilution, using a soft, low-hysteresis flexure in connection with an arm with a large momentum of inertia.[12,13] An alternative to mechanical-arm tiltmeters are the hemispherical resonating gyroscopes, which have recently reached sufficient sensitivity.[14] These gyroscopes, being built on glassy fused silica that contains no dislocations, are free of dislocation self-organized criticality noise. Gyroscopes of this kind will soon be tested in Virgo[15] for inertial controls of their seismic pre-isolators.

Back to the stone age

Following the insight acquired in Ref. 7, a non-metallic knife-edge hinge was designed to eliminate the dislocation self-organized criticality 1/f noise.

Tungsten Carbide was used as the ceramic material of the hinge in the tiltmeter presented here. It was chosen for its ease of cutting in suitable shapes by means of wire Electron Discharge machining.

This "novel" Tungsten Carbide hinge design is actually a modern version of a time-honored technique. Generations of scientists and engineers, charged to produce precision instruments to weigh gold and other precious materials, empirically learned to use hard stone knife-edge hinges in precision scales, so as to avoid systematic errors from metal hysteresis. The new understandings of dissipation in metals discussed in

Ref. 7 scientifically explain and justify that ancient empirical choice.

The paper is divided in the following parts. The engineering design of the tiltmeter prototype is illustrated first. Techniques considered and difficulties encountered to achieve sufficiently low systematic error in tilt sensing and rotational actuation are described. The option of interferometric sensing and its noise sources are discussed. Frequency tuning techniques and measurements showing that the knife-edge design has achieved an extremely low level of hysteresis, compatible with no hysteresis, in the hinge are shown. An upper limit of the sensitivity achieved with this knife edge is presented in a separate paper.[16] Finally, methods to further reduce hinge losses and improve ultra-low frequency angular sensitivity are discussed as well.

TILTMETER DESIGN

A horizontal, 205 mm long, 45 mm tall, 29 mm wide brass I-beam forms the tiltmeter illustrated in Figure 1. The arm carries two 45 mm brass cubes of 0.7 kg mass at both ends. Each cube carries a position sensor coil above and an actuator coil below. The sensors and actuators are symmetrically positioned at 125 mm distance from the hinge. Two small tuning masses are bolted on the side of each cube, and a small eccentric mass is placed on its outer surface, for coarse and fine adjustment of the center of mass height, respectively. The arm weight, including the cubes, is 2.4 kg; its momentum of inertia, disregarding the small contributions from the tuning masses and the coils, is 0.028 kg m^2.

A 45 mm long Tungsten Carbide wedge, with the tip positioned at the center of weight of the arm, supports the arm's weight. The knife-edge sits on a Tungsten Carbide anvil rigidly mounted in the tiltmeter box.

The tiltmeter is housed inside a 380 mm long, 150 mm tall, 120 mm wide aluminum box. Aluminum was chosen for its good rigidity and thermal and electrical conductivity. The box also supports the static components of the actuators and sensors.

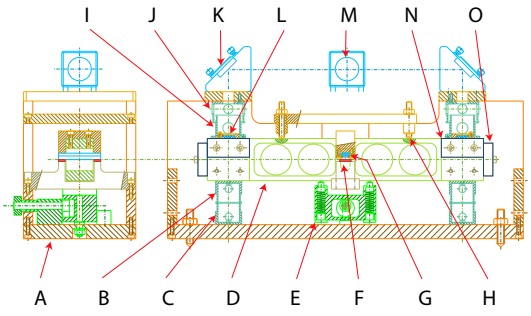

FIG. 1. Tiltmeter cross sections. A: Aluminum box, B: Secondary RF actuator coils (on arm), C: Primary RF actuator coils (on box), D: Tiltmeter arm, E: Lifting mechanism for transport, F: Tungsten Carbide anvil, G: Tungsten Carbide Knife-Edge, H: Seating (one of three) for the transport locks, forming a standard cone-slot-flat kinematic positioner, I: LVDT receiver coil, J: LVDT driver coil, K: Michelson relay mirror, L: Michelson end mirror, M: Michelson beam splitter mirror, N: Center-of-mass height adjustment masses mounted on both sides of the two main cube masses, O: Eccentric mass for fine tuning of center of mass height.

TABLE I. Sandwik Tungsten Carbide and Silicon Carbide properties.

Grade	Hardness		Transv. rupture strength	Compr. strength	Density
Units	Rock.–A	HV 30	Giga-Pa	Giga-Pa	g/cm^3
H10F	92.1	1600	4.3	6.25	14.45
6UF	94.3	2050	3.9	8.4	14.90
SiC			3.8	3.9	3.1

Tungsten Carbide wedge and anvil construction

The Sandwik grade H10F Tungsten Carbide chosen for the hinge is a 0.8 μm grain size sintered powder, cemented with 10% Cobalt. The Cobalt binder barely fills the interstices between grains, so that the grains are in direct contact to each other and the full rigidity of the Tungsten Carbide is available in compression. In these conditions, the material acquires characteristics similar to that of a polycrystal and the plasticity of Cobalt is expected to have no effect on dissipation. The H10F sintered aggregate has 92.1 Rockwell-A hardness, a compressive strength of 6.25 GPa and a density of 14.45 g/cm^3.

The Cobalt binder makes the aggregate electrically conductive, therefore workable by wire Electron Discharge Machining. The Sandwik grade 6UF, grain size is 0.4 μm would have been an even better choice (see Table I), but was not available in small quantities.

Particular care was necessary to produce the sharp knife-edge illustrated in Figure 2. It was found that to produce a good quality, sharp edge the two intersecting wire electron discharge machine cuts inside the Tungsten Carbide matrix must be completed before the body of the knife-edge is separated. If the edge is produced at the end of the cut, the stress accumulation fractures the material and a rugged edge is obtained.[17] A soft polish was necessary to remove small Cobalt debris and loose Tungsten Carbide grains left behind by the cuts. No other process was applied. The resulting edge was straight and, judging from electron microscope images (Figure 3), had a curvature comparable with the grain size (few μm). The 45 mm long knife edge protrudes 8 mm on each side from the 29 mm wide brass beam. The beam weight is supported on the two, 7 mm long, extreme sectors of the knife edge, resting on the support anvil. Assuming a 3 μm wide contact surface, the contact pressure is ~0.6 GPa.

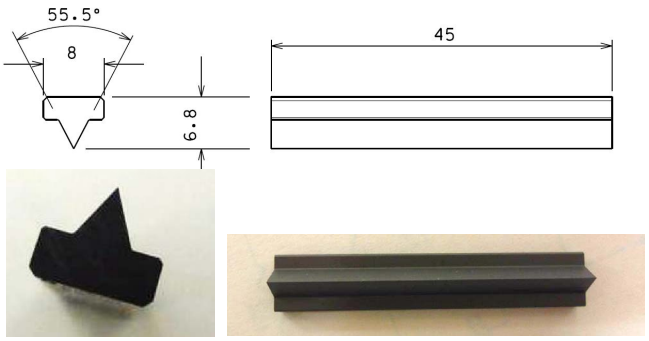

FIG. 2. Drawings and photographs of the Tungsten Carbide knife-edge. The units are millimeters.

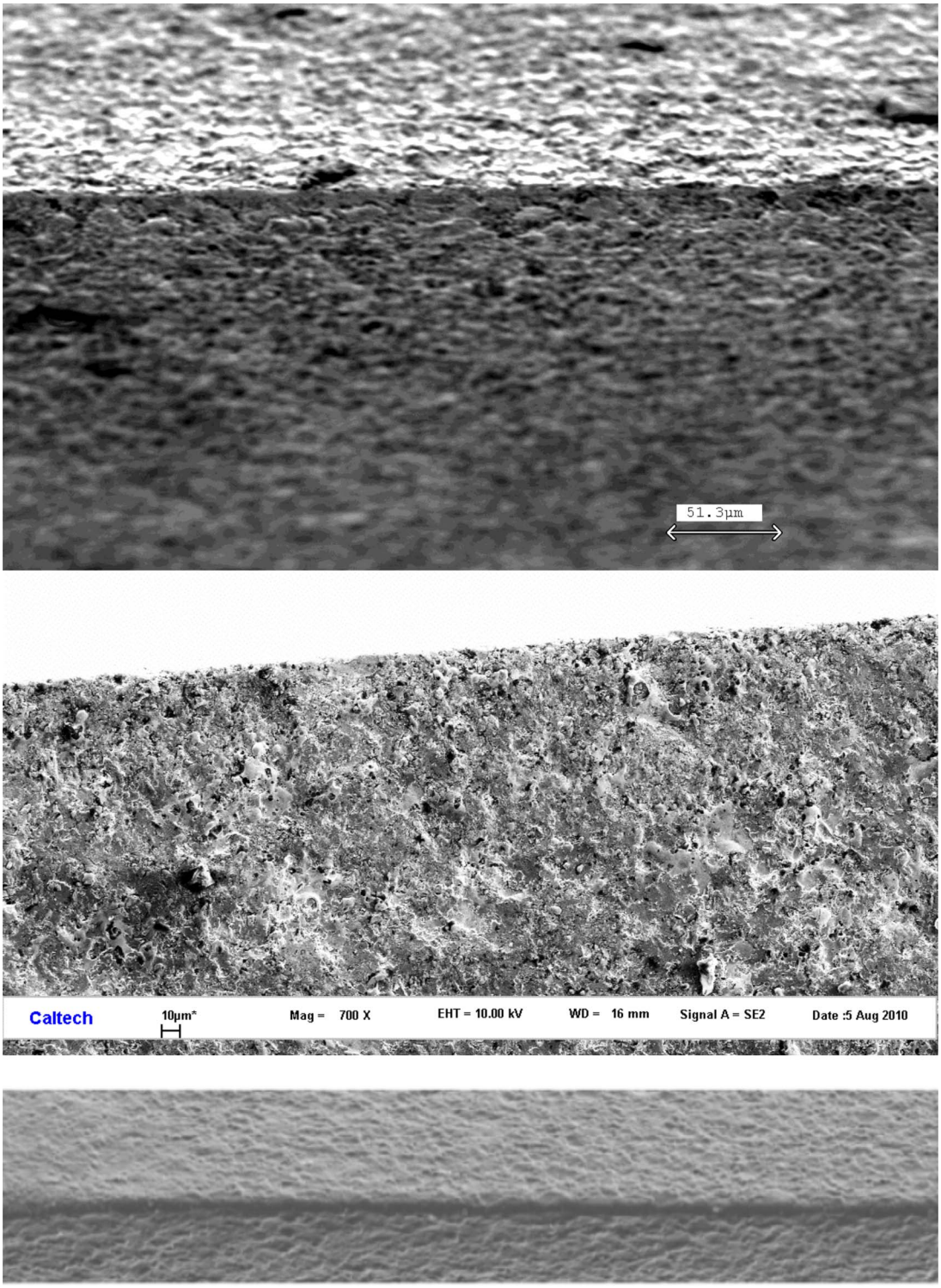

FIG. 3. Electron microscope images of the knife edge.

Locally, even higher stresses can be expected due to small misalignments, and asperities, while elastic deformation tends to reduce the maximum stress. The applied stress, well above the 345–485 MPa yield stress of Cobalt, peaks at even higher levels at the contact point between grains.

The plasticity of the Cobalt binder is therefore the limiting factor of the strength of the grain aggregate, and the cause of the difference of strength between the two formulations of Table I. The rather large angle, 55.5°, of the knife-edge in Figure 2 was chosen to form a wedge with sides below the critical slope that would have allowed the grains to slide and deform the edge. Because edge damage could be expected, the first care after initial operation was to check for signs of fractures in electron microscope images. Although a bright mark line was visible by eye on the anvil where the knife-edge rested, no other sign of damage, cracking or chipping on

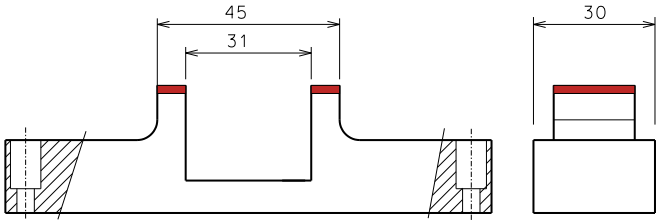

FIG. 4. U-shaped hinge-support anvil; the Tungsten Carbide plates are shown in solid color.

either side was observed on electron microscope images, even after accidental movements caused the knife edge to slide across the anvil.

The anvil, illustrated in Figure 4, was also made of Tungsten Carbide platelets brazed on a U-shaped Stainless steel support. The two platelets were co-polished on a precision grinding machine, to provide a perfectly co-planar support surface. Apart from the bright line, no sign of indentation was observed on the anvil surface.

A spare wedge with a 50 μm edge radius (the minimum that could be reliably controlled in the wire electron discharge machine used) was manufactured in case of damage to the sharp one, but it was never necessary. Wedges coated with diamond, diamond-like, Silicon Carbide, titanium oxide, titanium-nitrogen oxide, and other deposited glassy coatings listed in Table II were considered and manufactured to further strengthen the edge and reduce friction but, having found no damage in the uncoated sharp wedge, they were not used either.

Tiltmeter assembly

The tiltmeter and its case are shown during final assembly in Figure 5. The wedge simply sits on the anvil, without any transversal positioning. During transport and maintenance the beam rests on a lifting mechanism with four spring-loaded, spherical-tip pins actuated by an eccentric cam.

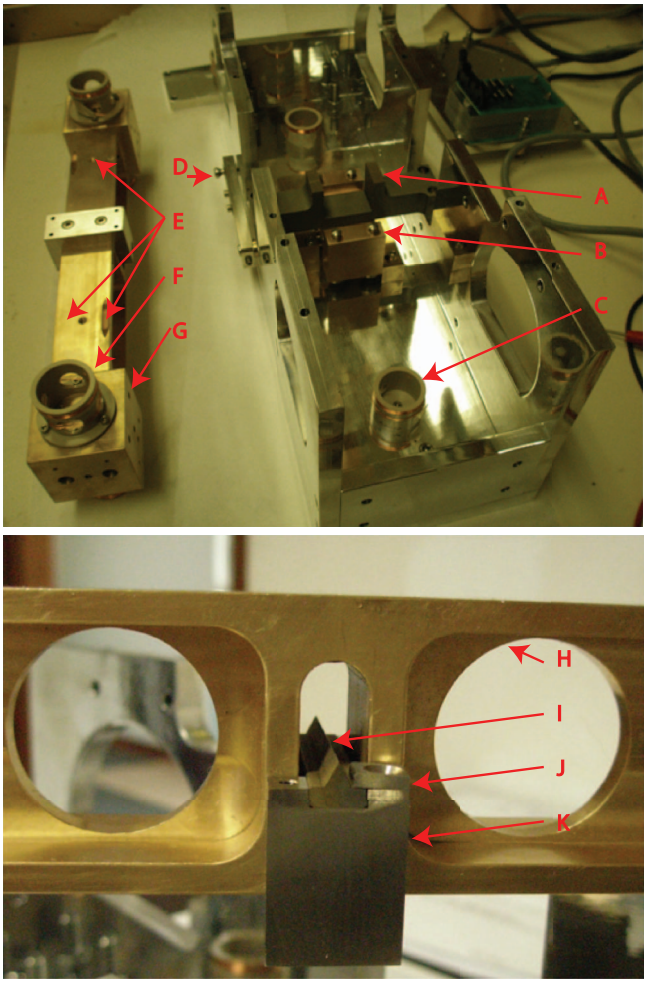

FIG. 5. Beam and case during final assembly (top), and close up of knife edge being clamped to the beam (bottom). A: Tungsten Carbide anvil surface, B: four-pin lifting mechanism block, C: lower (static) actuator coil, D: lifting mechanism arm, E: cone-slot-flat kinematic beam positioning, F: LVDT Driver coil, G: head mass, H: beam, I: Tungsten Carbide knife-edge, J: knife-edge clamp (one of four being mounted), K: knife edge bridge.

TABLE II. Physical properties of Lafer[18] coatings. Wedges and anvils with the marked with an asterisk (*) were manufactured. Only the naked Tungsten Carbide was actually tested on the tiltmeter.

Technical properties	CVD diamond	DLC CVD Lafer*	Carbon Lafer WC/C	TiN
Hardness: HV	10 000	2–4000	1200	2500
Friction coef.:	0,05	0,05	0,15	0,4
Coat T: °C	900	90–130	180	420
Work T: °C	600	400	380	520
Technology:	CVD	CVD	Magnetron	arc
Coating structure:	Monolayer	Monolayer	Multilayer	Monolayer
Lattice structure:	Polycrystalline	Amorphous	Amorphous	Single crystal
Technical properties	TiAlCN RedSpeed *	TiAlN Tinalox *	Tinalox plus	TiCN
Hardness: HV	3200	3500	3500	3000
Friction coef.:	0,25	0,4	0,15	0,3
Coat T: °C	450	450	450	420
Work T: °C	600	900	850	420
Technology:	Arc	Magnetron	Magnetron	Arc
Coating structure:	Multilayer	Monolayer	Multilayer	Multilayer
Lattice structure:	Single crystal	Single crystal	Single crystal-amorphous	Single crystal

When the lifting mechanism is "up," it presses the beam against three pins sticking down from the instrument cover, engaging into a cone-slot-flat kinematic mount machined on the top surface of the beam.

This kinematic mount provides the transversal positioning of the beam with respect to the case, the actuators and sensors. When the lifting mechanism is lowered to deposit the beam on the anvil, it transfers the positioning imposed by the kinematic mount. The spring strength of the lift mechanism was calculated for safe transport and maintenance of the instrument.

ACTUATION AND SENSING

Both sensing and actuation are strictly anti-symmetric with respect to the beam axis, built with identical components wired with opposite polarity on either end of the beam, thus being sensitive to angle and not to displacement, and generating pure torque and no net force.

Two options were considered for actuations and three for sensing.

For actuation we considered coil-magnet and coil-coil systems. The coil-coil actuator can be operated in AC mode to become completely insensitive to external magnetic fields. For sensing we considered standard LVDT position readout as described in Ref. 19, differential capacitive sensing and Michelson interferometer sensing.

Large windows were opened in all coil spools to mitigate the piston-damping effect when operating the tiltmeter in air.

While the tiltmeter is designed with a ceramic knife-edge to be free of metal elasticity noise, the electrical wiring is forcedly metallic. Obviously stranded wires cannot be used because of the stick and slip noise between the strands. Therefore, although stiffer, solid wires were used. The poor quality factor of OHFC (Oxygen Hydrogen Free Copper) and of polyhimide coating would have introduced relatively large losses. Normal polyhimide-insulated OHFC wires were used initially; they were replaced with naked 100 μm Copper Beryllium wires for the last measurements. To minimize the contribution to hysteresis and elasticity noise from the wires, the wires leading from the beam to the case were small loops made of thin wire, soldered on pad pairs on printed circuit boards bolted as close as possible to the hinge axis. Even in these strongly diluted conditions, the hysteresis of the wire is thought to contribute not negligible losses to the instrument.

Actuation

Actuation is necessary for feedback operation of the tiltmeter, and is very useful in the characterization phase.

The coil-magnet actuator is simpler, but nominally identical magnets can differ in strength by several percent, thus resulting in net forces. Additionally coupling with Earth's or man-made magnetic fields can generate unacceptable torque on unequal magnets. For this reason the coil-coil actuators were preferred despite the additional two wires leading to the arm.

In the coil-coil actuator, the pair of coils mounted on the beam is wired in series, with the same orientation to avoid generating spurious torque from coupling with Earth's and other ambient magnetic fields. They are faced by a pair of matching coils mounted on the case, which are also wired in series, but oriented with opposite field. This configuration generates pure torque and no force on the beam.

The coils can be operated either in AC or DC mode. The AC mode generates no static torque even in connection with external magnetic field gradients. In the AC mode, the same sinusoidal signal is sent to both on-beam and on-case coils, with fixed amplitude on the on-beam pair and amplitude modulation on the on-case pair.

The actuation torque is proportional to the product of the currents in the two circuits. The maximum torque available is limited by the fixed-amplitude excitation of the on-beam coils, which is kept to a minimum to minimize heating and spurious couplings.

The tests reported in this article were made with coil-coil actuation.

Due to the 1/f electrical noise of electronic circuits, it was difficult to generate coil actuation voltages with sufficiently low noise at very low frequency. Due to this problem, the low-frequency high-sensitivity measurements in Ref. 16 were made without actuators. Suitable high-stability current generators need to be developed for low-noise-low-frequency feedback operation.

Capacitive sensing

Differential capacitive sensing requires a pair of gap capacitors on each side of the beam, wired in an AC Wheatstone bridge fashion. High sensitivity can be achieved with capacitive sensing, but with two disadvantages. The second order effects of the electrostatic excitation generate strong nonlinear torques, which tend to destabilize the tiltmeter. There is no simple way to avoid strong air damping between the capacitor gaps. Therefore, capacitive sensing was abandoned.

LVDT sensing

The initial measurements reported in this paper were made with a single primary coil LVDT, as described by Tariq.[19] LVDT sensing was found to generate weak stray forces, through eddy current repulsion on the case walls. This effect was observed as a small beam resonant frequency shift when changing the LVDT primary excitation voltage. To eliminate the eddy current effect, leakage-field-compensated primary and secondary coils with nulled magnetic field on the case were designed. In the original design the RF-emitting primary had a single coil. The two additional coils, each with half the turns and counter-wound with respect to the central one, null the radiated magnetic field on the instrument case while still generating strong position signal on the secondary. The compensated LVDT design is described in Ref. 16.

INTERFEROMETRIC SENSING

A Michelson interferometer is a virtually force-free, wireless, and intrinsically differential position sensor, with

demonstrated sensitivity better than 10^{-13} m[20] in fringe counting mode; theoretically it is ideal for tiltmeter readout. The Michelson readout is already used in torsion pendula[21] and is potentially superior to the LVDT sensors. A prototype of the interferometer for the tiltmeter was developed to identify the dominant and potential noise sources at low frequency, and then tested. It was found that a successful implementation of an interferometric readout requires the solution of a few technical problems.

The first issue is alignment – the optical layout has to be able to cope with the tilt of the beam. The second problem is that the frequency drift of a non-frequency stabilized laser, coupled to an uncorrected small optical arm imbalance, easily produces unacceptably large low frequency position measurement noise. At low frequency this noise is in excess of what could be achieved with the LVDTs. Laser power fluctuations are an additional limitation.

Suitable solutions could be identified for all the problems found, but not having the resources to implement them, the interferometer could not be used. The design and tests of this interferometer prototype are reported in this section to illustrate the problems still to be solved. The characterization of the tiltmeter reported here, as well as the high sensitivity measurements reported in Ref. 16 were performed with LVDTs.

Interferometer alignment requirements

The problem of interferometric angle measurement and mirror tilt immunity in Michelsons has been already treated in literature using corner cubes or cat's eyes retro-reflectors.[21,22] To minimize complexity, it is important to determine whether retroreflectors are actually required in this application.

Standard Michelson interferometers tolerate large arm length imbalances but two effects degrade fringe visibility in a tiltmeter. As the target mirrors tilt, the beams are misaligned by twice the tilt angle and move in opposite directions on the beam splitter plane. If the movement is large compared with the spot diameter, the overlap of the two returning beams will reduce, generating less interference visibility. Additionally, if the phase shift across the spot becomes larger than $\frac{1}{2}$ wavelength, the circular patterns turns into straight fringes on the detector plane. The fringe becomes narrower as the tilt increases, eventually compromising the visibility on the photodiode.

Figure 6 shows a simplified diagram of the tiltmeter readout interferometer. The main beam, incoming perpendicular to the drawing plane, is divided at point O by a beam splitter into the arms of the interferometer. Each arm is routed onto its own target mirror on the tiltmeter arm. Fringe visibility is not an issue once the interferometer is locked at the null tilt position. To ensure tiltmeter startup it is necessary that the maximum mechanical tilt does not seriously compromise the fringe visibility. The visibility will be satisfactory as long as the thickness of the fringes is larger than the width of the overlapping area on the detector. Figure 7 shows the principal ray of each beam propagating back from the target mirror onto the plane of the detector where the interference takes place. It is easy to show that the intensity of the interference pattern at

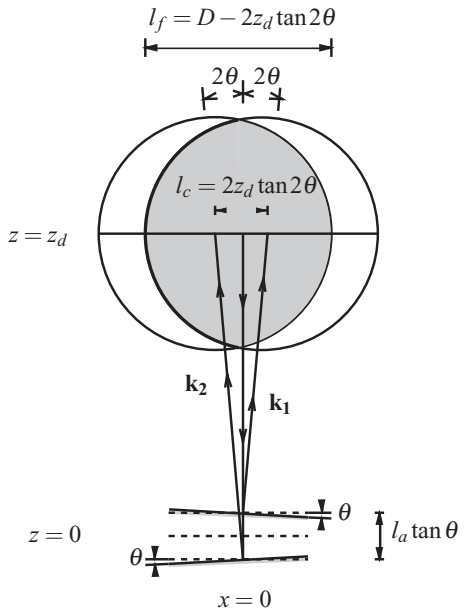

FIG. 6. As the target mirrors tilt, the beams move in opposite directions on the beam splitter plane.

any point whose horizontal coordinate is x can be expressed as

$$\mathrm{I} = 2\{1 + \cos[2\mathrm{k}(\mathrm{x}\ \sin(2\theta) - \mathrm{l_a} \tan\theta\ \cos(2\theta))]\}, \qquad (1)$$

where k is the wave number, θ is tilt angle of the tiltmeter, and $\mathrm{l_a}$ is the distance between the interferometer arms. From expression (1), the width Δx of the straight fringes can be calculated by setting the equation $2k\Delta x \sin 2\theta = 2\pi$, which, by introducing the value $\mathrm{k} = 2\ \pi/\lambda$, can be written as $\Delta x = \lambda/(2 \sin 2\theta)$.

The maximum allowable angular displacement can be calculated by solving the equation $\Delta\mathrm{x} = \mathrm{l_f}$, where $\mathrm{l_f}$ is the width of the overlapping area. In terms of the angular displacement θ, the diameter of the beam D and the distance $\mathrm{z_d}$ from the mirror to the detector, the equation is

$$2[\mathrm{D} - 2\mathrm{z_d}\ \tan(2\theta_\mathrm{m})] \sin(2\theta_\mathrm{m}) - \lambda = 0. \qquad (2)$$

The input optics was designed to produce light spot diameters of 4.8 mm on the mirrors, beam splitter, and

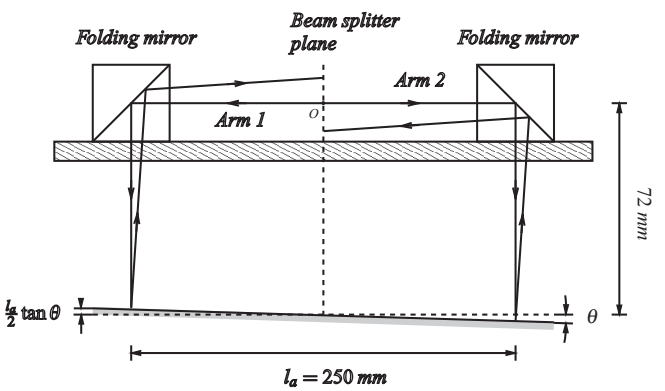

FIG. 7. The width of the straight fringes should not be smaller than the width of the overlapping area of the beams on the photodiode plane.

photodiodes. For a distance $z_d = 30$ cm and a wavelength $\lambda = 632.8$ nm, the maximum acceptable displacement is $\theta_m = 33.1$ μrad. This corresponds to a linear displacement of approximately $\theta_m\, l_a/2 = 4.2$ μm, well below the maximum angular displacement of 4 mrad determined by the mechanical end stops.

Retroreflectors are therefore necessary. Cat's eyes allow up to $\pm 1^\circ$ tilt,[21] more than the tiltmeter requires.

Angular noise identification

Figure 8 shows the implementation of the Michelson interferometer. Ambient vibrations and acoustic noise, identified by correlation with the accelerometer signal on the table, dominated the signal at frequencies between 1 Hz and a few kHz.[22] At frequencies between 1 Hz and 200 mHz the sensitivity was limited by laser intensity noise, and below 200 mHz the dominant contribution was likely laser frequency noise. Acoustic noise and spurious vibrations will be mitigated in the operational environment of the tiltmeter. To achieve sensitivity at lower frequencies, laser frequency and power fluctuations need to be mitigated.

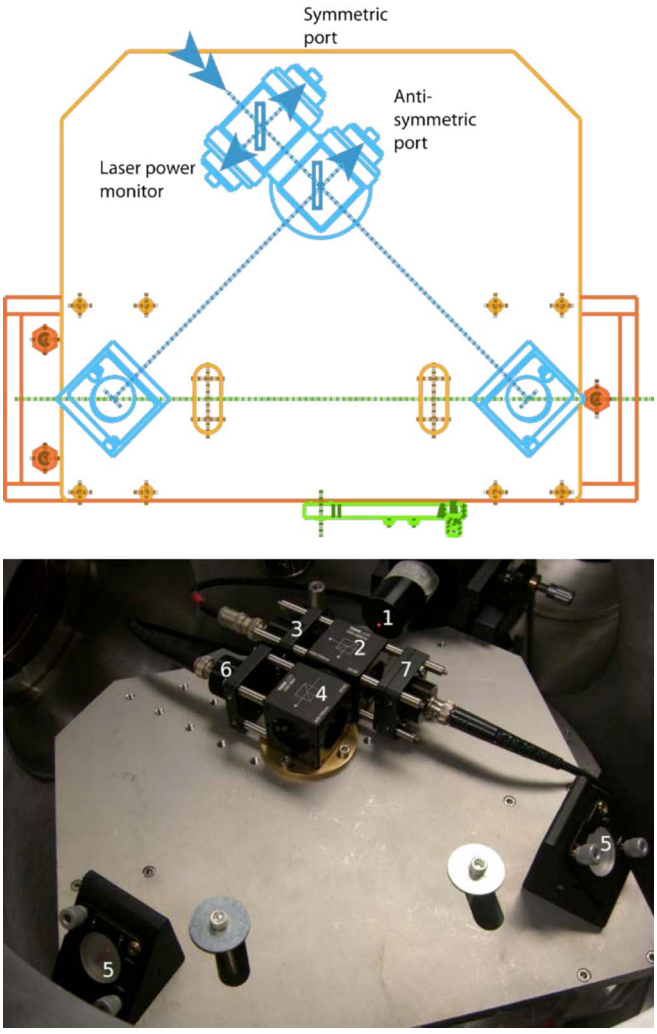

FIG. 8. Michelson interferometer scheme and prototype. The Michelson is designed to be mounted on the case cover, with the split beams folded down to the tiltmeter beam by the two 45° mirrors.

Power fluctuation noise reduction

The effect of laser power fluctuations is a well-known problem in interferometers using one or two interference sensors.[23] The reduction of intensity noise can be accomplished by using a power stabilized laser or by normalizing the signal with a third interference sensor[23] in reversible fringe counting mode. Either, or a combination of both techniques, would easily reduce this noise source below the tiltmeter requirements.

Frequency noise reduction

A light frequency linewidth of 10 MHz typical on common solid state lasers, coupled with an arm imbalance of just a fraction of a mm is sufficient to produce the observed level of measurement error. Although it is possible to implement frequency stabilization in a laser, such an approach falls out of the span of the tiltmeter project. A possible mitigating strategy is to use a distributed feedback laser diode with temperature control.[24] This type of laser diodes incorporates a diffraction grating element that allows the selective generation of light within a narrow frequency linewidth. The distributed feedback laser (used in Ref. 21) produces light at a wavelength of 1550.9 nm with a typical frequency linewidth of 2 MHz.[25] Other proprietary technologies are capable to supply a frequency linewidth of as low as 50 kHz.[26] These devices, developed for long-haul telecommunication systems to minimize the chromatic dispersion in optical fibers around 1550 nm,[25] are already available at accessible prices. Thermal fluctuations of the in-cavity grating may still limit the stability of the line, and thus the low frequency performance of the tiltmeter.

Operation on equal-arm-length fringe to eliminate frequency noise

The Michelson's frequency noise can be entirely removed if the interferometer is operated at or around the equal-arm-length fringe where the laser frequency noise becomes irrelevant. Once the central fringe is identified, the optical arm imbalance can be easily nulled by means of the tiltmeter feedback actuators. The problem is that fringe-counting mode operation used for displacement measurements requires coherent laser light. This light makes the interferometer insensitive to arm unbalance and therefore it is difficult to identify the central fringe that eliminates the frequency noise. Perhaps the simplest method to identify the central fringe while operating in fringe counting mode is to mix white light with the high coherency laser light. The fringe visibility is reduced everywhere, except for the central fringe and the visibility spike clearly identifies the central fringe. Once identified, the tiltmeter feedback mechanism simply locks the tiltmeter arm to that position and the white light source can be switched off. The central-fringe-finding mechanism, although simple, could not be tried in the interferometer prototype because it was never coupled with the tiltmeter mechanics.

MECHANICAL FREQUENCY TUNING AND ARM LEVELLING

Conceptually, a tilt accelerometer can work with arbitrary arm orientation; only the dynamic changes of the arm position with respect to the case are true angular acceleration signals. Historically, tilt accelerometers have been designed with both horizontal and vertical arm, or even instruments that work in both configurations.[10,27] The use of a knife-edge hinge requires near perpendicularity of the knife-edge with respect to the anvil it rests on. The limited range of sensors and actuators impose even tighter limits (<1 mradian) on the angular positioning of the tiltmeter arm. With no elastic restoring force provided by the knife-edge, the only solution that provides stability, i.e., positive resonant frequency, is when the center of mass is positioned at a distance δ below the hinge. The arm tilt resonant frequency ω will be

$$\omega = 2\pi f \sqrt{\frac{Mg\delta}{I}}, \tag{3}$$

where M is the arm mass.

If $\delta = 0$ the tilt accelerometer is totally insensitive to horizontal acceleration.

If $\delta \neq 0$ the tilt accelerometer senses linear acceleration a_x as an apparent tilt acceleration

$$\alpha = \tau/I = \delta\, M\, a_x/I = (\omega^2 a_x/g). \tag{4}$$

A typical tilt accelerometer tuned at 50 mHz and subject to linear acceleration a_x will sense a false angular acceleration

$$\alpha = 0.012\, a_x. \tag{5}$$

As a comparison, an ideal horizontal accelerometer, in addition to actual linear acceleration, senses any tilt as an unwanted linear acceleration term

$$a_{\theta x} = \theta g, \tag{6}$$

where $g = 9.8\ m/s^2$ is Earth's gravity acceleration.

The key point is that, because a tilt accelerometer with small δ is naturally insensitive to linear acceleration, its signal can be used to diagonalize out the unwanted tilt term from a linear accelerometer signal up to the limits of the tilt accelerometer sensitivity and vice versa, eliminating the linear acceleration component from the tiltmeter signal. The optimal choice of δ depends on the instrument's use, keeping in mind that above resonance the tilt accelerometer measures rotation with respect to the inertial frame, and below resonance the rotation is measured with respect to Earth gravity. Note that the easiest way to measure δ is to insert the resonant frequency ω in the formula

$$\delta = \frac{I\omega^2}{Mg}, \tag{7}$$

where δ grows rapidly with ω; at 0.5 Hz (used in Ref. 16), δ is already 12 mm. A relatively large δ may be advantageous if the instrument is used as an absolute tiltmeter, but the smallest possible δ should be used if the instrument is intended as a tilt accelerometer.

In both cases, the quality of the instrument and its ultimate sensitivity depend on the dissipation losses of the hinge, which is the only unavoidable point of entry of all noise forces. Hysteretic losses are especially noxious because they produce a persistent signal indistinguishable from a constant angular acceleration. A tiltmeter sensitivity of $\sim 10^{-10}$ radian/$\sqrt{\text{Hz}}$ was measured in this instrument in a higher frequency configuration.[16]

Tuning δ to low values is relatively easy, adding small masses either above or below the center of mass of the arm. The difficulty when tuning δ very close to zero is that the restoring torque τ,

$$\tau = K_t\theta = Mg\delta\theta \tag{8}$$

drops with δ and the necessary arm leveling becomes progressively difficult. To illustrate this difficulty, at 50 mHz the angular spring constant K_t is just 0.0028 Nm/radian; to balance the beam within 0.1 mradian the torque must be adjusted to within $\sim 0.3\ \mu$Nm, i.e., positioning 3 mg with the position of 0.1 mm. The arm of the prototype was manually balanced by moving masses of a few mg along the top surface of the arm. Below 50 mHz, the perturbation of opening and closing the enclosure was more than the correction itself and a "closed-box" remote manipulation mechanism becomes necessary.

Of course the arm can be leveled using the electromagnetic actuators, to apply a static corrective torque. This was done when the tiltmeter was actively tuned below 50 mHz, but the high torque required has the price of injecting actuation noise. A remote manipulator should be designed and implemented for arm balancing, if resonant frequencies are below 50 mHz.

THERMAL AND AIR CURRENT SHIELDING

The tiltmeter is very sensitive to air currents, and differential thermal fluctuations. It was positioned on top of a 1.2 $\times$ 1.2 m optical table, mounted on strong steel footings, on the basement floor of the West Bridge building at Caltech. The table was situated in the corner of the room farthest from the door, against the side of the building. The entire table was enclosed in a 5 cm thick, rigid, Styrofoam box, sealed with polyurethane adhesive foam in all corners except for the access panel, which was provided with an overlapped lip seal. The tiltmeter was further enclosed inside two concentric, rectangular, aluminum boxes placed upside-down on the optical table. The aluminum walls of the boxes were 3 mm thick, each enveloped within a 2.5 cm thick, soft rubber foam layer for further thermal and acoustic isolation. All electronics and power generating equipment were located at least one meter away. Long-term stability tests were performed operating the data acquisition remotely, with the laboratory doors locked.

DATA ACQUISITION

The initial measurements reported in this paper were done using a National Instrument/Labview control and data acquisition system. When the sensitivity and response time limits of this system were reached, a new evolving acquisition control system, discussed in detail in Ref. 16, was developed and implemented. The points at which the system change took place are specified in the discussions below. The progressively improving noise performance is discussed where relevant.

MECHANICAL FREQUENCY TUNING

The resonant frequency of the tiltmeter can be changed in two ways: mechanically, by changing the height of the arm's center of mass with respect to the hinge point, and dynamically by feeding the LVDT signal to the actuators with a suitable linear gain, thus generating an electro-magnetic spring of arbitrary strength.[28]

For each mechanical setting, frequency-versus-gain measurements were performed by remotely changing the resonant frequency via the feedback gain. The data followed precisely the expected square root law, as a function of both electromagnetic and mechanical frequency tuning, as shown in Figure 9. The lowest resonant frequency that could be reliably achieved by purely mechanically means was ∼50 mHz. Resonant frequency as low as 10 mHz could be reached dynamically, as illustrated in Figure 9.

For each electro-mechanical setting the oscillation was excited and the ringdown fit with a damped sinusoid function to extract the quality factor of the oscillation. Only the lowest amplitude section of the oscillation was taken into account in the fitting. The quality factor data are plotted in Figure 10. At same frequency values, data points taken with the feedback switched off showed higher quality factors, indicating that the

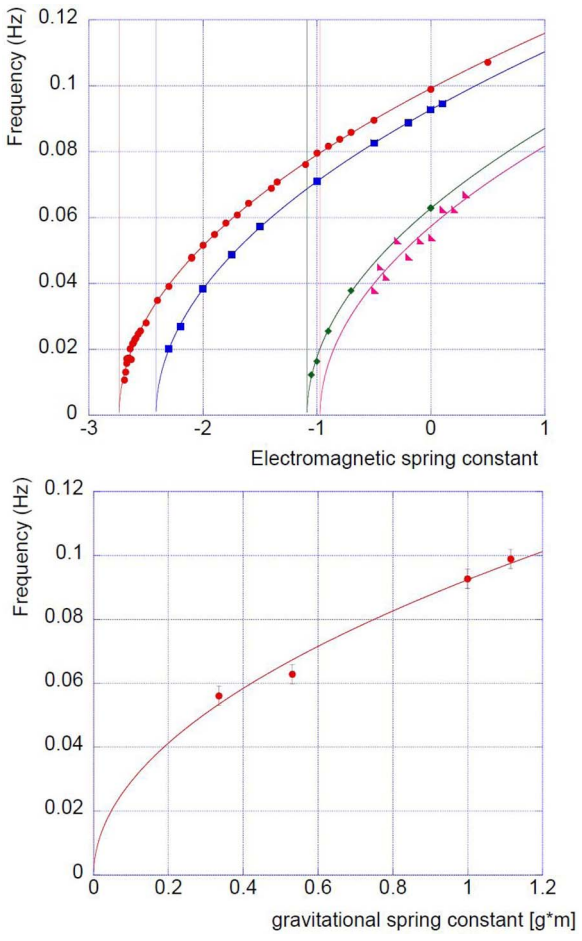

FIG. 9. Resonant frequency versus feedback gain in arbitrary units (top) for four different mechanical center of mass height settings and for the four settings without feedback (bottom). For each of the data sets, the data were fit with the function: $a \times \sqrt{(k_s - b)}$. The error bars (shown on the bottom curve only) have been estimated from the spread of repeated measurements at the same settings.

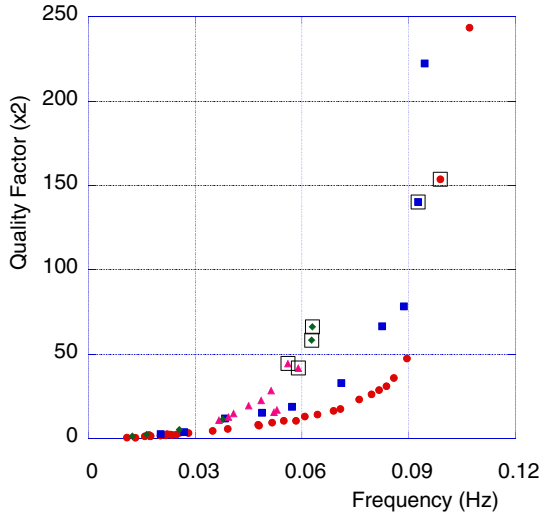

FIG. 10. Quality factor in air of the resonance as function of frequency for different gravitational and electromagnetic spring constants. The gravitational spring constant is: Circles: 1.11 [g m], Squares: 0.999 [g m], Diamonds: 0.531 [g m], Triangles: 0.335 [g m]. The boxed points are the same of Figure 9, bottom, with electromagnetic spring switched off.

Labview control system introduced spurious losses dominating the measured values. System inspection later showed that the Labview produced the feedback signal with a delay of 100 ms. Following this observation, the custom data acquisition and control system was put into use. For quality factor measurements, only the measurement points with the feedback off (boxed points in Figure 10) can be trusted at high frequency. At very low frequencies (below 30 mHz) the losses introduced by the feedback delay become irrelevant with respect to mechanical losses, and the data points of the four different data sets overlap.

HYSTERESIS MEASUREMENTS

Hysteresis in metals is the harbinger of dislocation entanglement, leading to Self-Organized Criticality 1/f noise; it set the sensitivity limit of tiltmeters. It is therefore a key measurement; the following considerations are relevant. This tiltmeter was designed with a ceramic knife-edge rather than a metal flexure, specifically to avoid the 1/f noise resulting dislocation entanglement in the latter. Ceramic hinges will have their own hysteresis sources. Any stick-slip process will produce hysteresis, and rotation on the granular structure of the Tungsten Carbide edge can be expected to stick-slip. At any given time, the hinge rests on a given set of grains. During rotation the hinge will continuously switch to different sets of grains, but for sufficiently small oscillations, the hinge will remain on a given set of grains, with the oscillation causing only variations of the elastic compression of the ceramic crystals supporting the weight. Please note also that the Cobalt binder in the sintered Tungsten Carbide was less than the amount necessary to completely fill the gaps between the ceramic grains. Because it is ductile, it can be expected to be completely squeezed out of the contact points between grains and simply form "crowns" around the contact points that keep the Tungsten Carbide grains from slipping. The binder will be squeezed out most efficiently in the areas of maximum

stress, i.e., the hinge point (which may account for the discoloration observed on the contact line on the anvil). Therefore, after a rapid initial settling, it can be expected that the Cobalt binder will contribute negligibly to the mechanical losses. If the above considerations are correct, the hysteresis from the stick-slip mechanism of large oscillations should shut down for small oscillations.

One should not forget that some hysteresis is contributed by the electrical wiring between the case and the arm.

It is therefore very important to quantify and characterize the hysteresis at different oscillation amplitude levels. The measurements show less hysteresis than what may be expected with metal flexures in comparable geometries. What is even more important, the fractional hysteresis is found to decrease, and may even vanish altogether, with the small excursion amplitudes typical for quiet seismic conditions. This may remain true even in high tilt noise environments, if the tiltmeter is operated in feedback, as long as the feedback impedes large hinge excursions.

It should be noted here that other sources of hysteresis are possible, induced by load changes in capacitors and semiconductors of both driving and sensing electronics. Drift of amplifier gains and of the reference voltage in the ADC, as well as changes of atmospheric pressure and temperature are also factors that can produce systematic errors in the measurement. These effects may cause some of the observed hysteresis, or may even accidentally compensate and reduce some of the observed effect. Even more care was spent in Ref. 16 to minimize these effects while providing a more significant statistical evaluation of the instrument performance than what was possible with the data presented in this paper.

Measurement method

To study the hysteresis' behavior, the following experimental procedure was performed.

The tiltmeter actuators were used to apply a torque pulse with a full period (t changing from 0 to 2 π) of the function:

$$\tau = \alpha(1 - \cos(\omega t)). \tag{9}$$

This pulse shape was chosen to minimize the excitation of the oscillation mode of the arm; the frequency chosen to generate the pulse, $\omega = 5$–10 mHz, was several times slower than the resonant frequency. After the end of each excitation pulse the tiltmeter is monitored for 200–300 s before the next excitation, which is then applied with the opposite sign of α. The hysteresis is evaluated by comparing the response to positive and negative excitations after at least two cycles.

Three experiments were performed at progressively decreasing excitation excursions ranging from 3 mradian in the first test, 137 μradian in the second and 390 nradian in the third.

Large amplitude: 3 mradian range

The tiltmeter was mechanically tuned at 58 mHz. The static hysteresis was measured for different values of α with arm oscillation amplitudes ranging from ± 0.4 mm to ± 0.05 mm. The hysteresis measurement was performed by simply recording the tilt reached just before the next pulse.

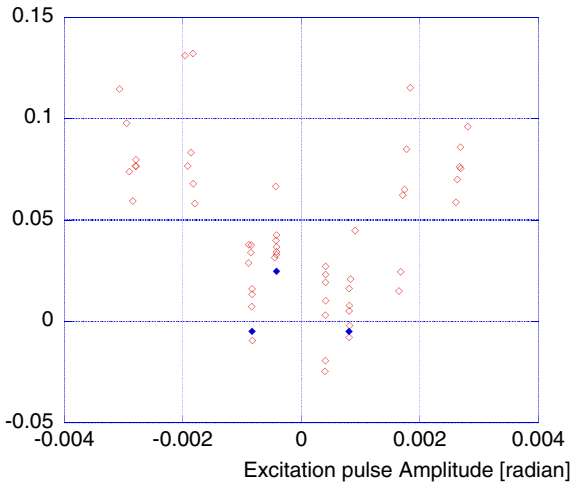

FIG. 11. Fractional hysteresis versus amplitude scans performed with electromagnetic spring feedback turned off. Empty diamonds, ±3 mradian amplitude scans, each representing a single measurement; positive and negative measurements are alternated. Full diamonds, ±1 mradian scan, each diamond is an average of more measurements performed at the same amplitude.

The measurement (Figure 11) shows a non-uniform hysteresis, as large as 10% for large excursions. The fractional hysteresis observed was smaller for smaller excitation pulse amplitude. The points taken between ± 1 mradian were compatible with no hysteresis within the measurement scatter. The points with larger amplitude show clear fractional hysteresis.[17]

After this first hysteresis test, the National Instruments/Labview control and data acquisition system were abandoned and the increasingly precise custom system used from this point onwards.

Intermediate amplitude, 137 μradian range

In the intermediate amplitude hysteresis measurement, the amplitude α of the excitation was $\alpha = \pm 0.075$ V. It generated rotational signal pulses 17 μm on the LVDT, or 137 μradian of tilt. The mechanical resonant frequency was tuned at 31 mHz. The data are shown in Figure 12. A

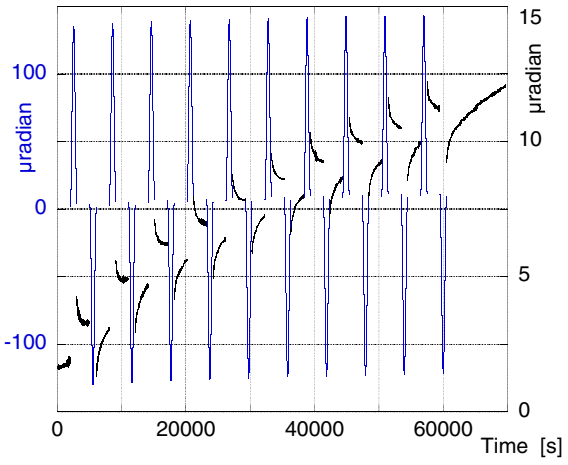

FIG. 12. Excitation pulses (left scale) and angular relaxation (right scale) of the tiltmeter, raw data.

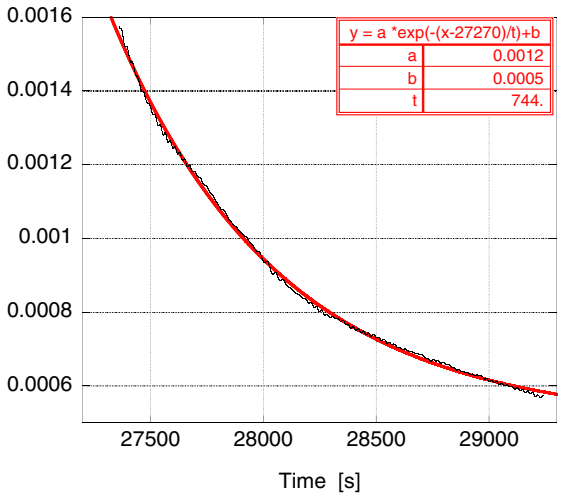

FIG. 13. Fit to one of the 20 relaxation curves.

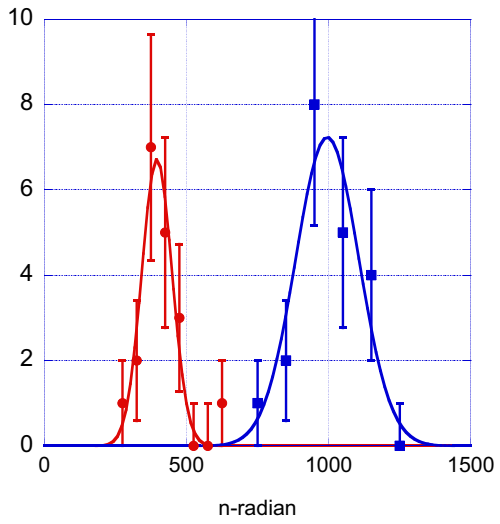

FIG. 14. Measured Hysteresis (circles) and Anelasticity (squares) with 137 μradian excitation excursion. The Gaussian fits give a hysteresis of 369 ± 7 nradian with a Gaussian width of 75 nradian, and anelasticity of 955 ± 23 nradian and a width of 157.

$\sim$10 μradian tilt drift was observed during the 20 h-long experiment. Small day-night and seasonal building tilt oscillations are not surprising because the sun heats the building from different directions (see also Figure 16 in Ref. 16) and ground swells with changing ambient humidity. Similar daily oscillations, as well as tilts connected with rainy and dry periods, were observed in the nearby Synchrotron building. Additional drift may have been contributed by slow relaxation of stress in the four OHFC electrical wires. The recorded drift was amplified by the very low frequency tune of the arm. A second order polynomial was sufficient to correct the drift in the data.

Hysteresis and anelasticity are clearly visible, they are evaluated by fitting the relaxation after the end of each excitation pulse with an exponential decay function

$$a + b\, e^{t/\tau}. \tag{10}$$

An example of this fit is shown in Figure 13. The amplitude b of the fitted exponential is a measurement of anelasticity with an observed relaxation time τ, while the changes of the level a are used to measure the static hysteresis. Static hysteresis was evaluated as the half-difference between the two a terms of two consecutive excitation pulses. The results are summarized in Table III and in Figure 14. The measured anelasticity lifetime τ was between 600 and 1200 s, averaging 800 s. The exponential function does not always fit the data as well as in Figure 13; the data have a tendency towards a longer τ lifetimes when the fit is restricted to the final part of each segment.

TABLE III. Measured hysteresis and anelasticity with 137 μradian excitation excursion.

Units	Hysteresis (nradian)	Anelasticity (nradian)
Mean	404	998
Standard deviation	78	104
Standard error	18	23
Excitation	137 000	
Fractional effect	0.0029	0.0073

Small amplitude, 390 nradian range

In the third test, the amplitude of the excitation was the smallest, $\alpha = \pm$ 182 μV, generating $\sim$390 nradian of tilt with a 10 V/mm calibration. The resonant frequency was 86.83 mHz. The test was performed at night-time run, inside a multiple layer Russian doll shielding. The data presented a smaller tilt drift, which this time was de-trended by subtracting a fourth-order polynomial. The polynomial correction, fit to the data outside the excitation periods, had a total excursion of 2 10^{-5} V (i.e., $\sim$2 nradian).

The data acquisition was disturbed by two small seismic events at time $\sim$8600 and $\sim$9700 s, see Figure 15.

The hysteresis measurements, from time 0 to 8500 s are discussed first. The relaxation data were plotted in Figure 16. The data are shown in Table IV: Measured Hysteresis and Anelasticity with 137 μradian excitation excursion. With the smaller excitation of this test laboratory and data acquisition noise and/or drifts dominated the signal during the relaxation periods. No anelasticity behavior was visible. Therefore, each relaxation data segment between two consecutive, alternate-sign excitation pulses was simply averaged. Hysteresis is expected to have the same sign of the preceding excitation pulse; therefore, the average value of each segment was multiplied

TABLE IV. Measurement of hysteresis with the 390 nradian excitation pulses. The first error of the fractional hysteresis is the standard deviation, and the second the standard error.

Relaxation time sections	Control	Excitation sign included
Data points	18	18
Hysteresis mean (μV)	**−0.01**	**0.43**
Standard deviation (μV)	0.62	0.44
Standard error (μV)	0.15	0.10
Excitation amplitude (μV)	364	
Fract. hysteresis	$0.0 \pm 1.7 \pm .0.4 \times 10^{-3}$	$1.2 \pm 1.2 \pm 0.2 \times 10^{-3}$

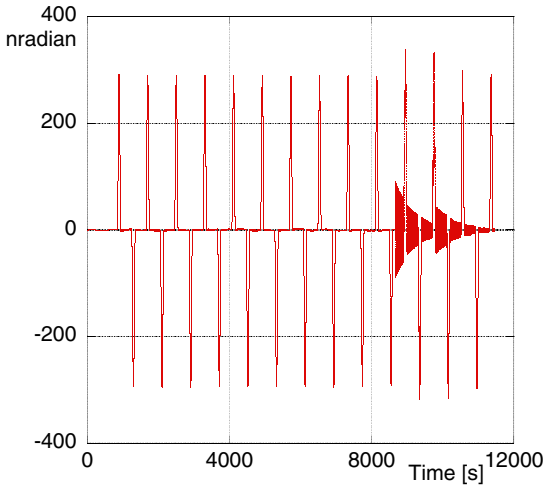

FIG. 15. De-trended data of hysteresis measurement for very low excursion excitation (37 nradian).

by the sign of its preceding excitation in column 3 (and Figure 16). The same values without sign multiplications, listed in column 2, were used as controls to evaluate systematic errors.

The seismic events interrupted the hysteresis measurement, but helped illustrate the quality of the hinge.

When the excitation sign is taken into account, the mean hysteresis signal (bolded in Table IV to indicate importance) is $0.43 \pm 0.44 \pm 0.10\ \mu$V, where the first error is the standard deviation of the data points and the second is the standard error. The hysteresis value is within the standard deviation range but significantly positive. The control set (same data without alternate sign correction) gave a value of $-0.011 \pm 0.62 \pm 0.15\ \mu$V.

The fractional hysteresis taking into account the excitation amplitude was $1.2 \pm 1.2 \pm 0.27 \times 10^{-3}$.

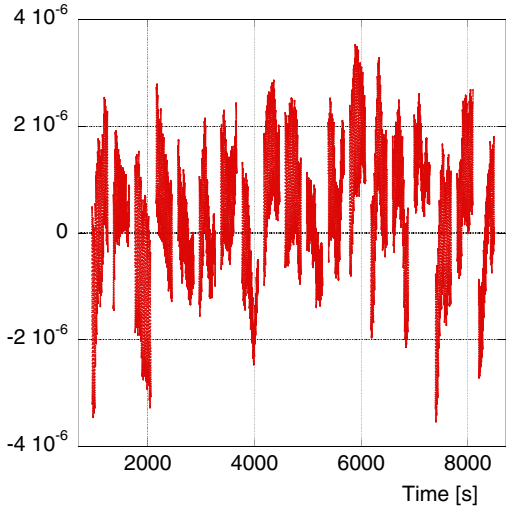

FIG. 16. Relaxation segments of 18 hysteresis measurements made after 390 nradian excitation pulses of alternate sign. The vertical scale is in Volts. Each data segment in this plot is multiplied by the sign of its excitation pulse so that the hysteresis effects will have positive sign.

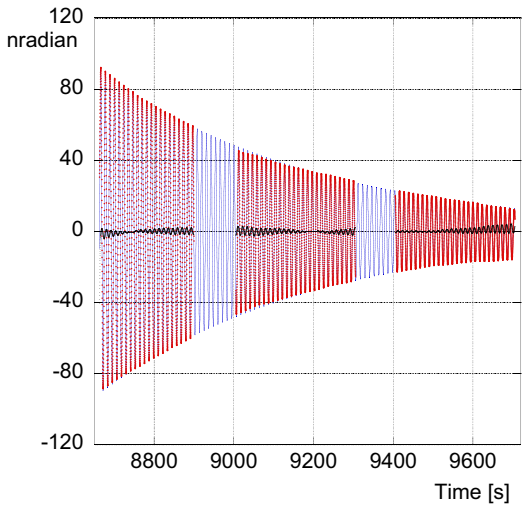

FIG. 17. Excitation after first seismic event, the data are shown in red, with a damped sinusoid fitting, in blue. The data during the excitation pulses are excluded; the fit extends coherently across two excitation pulses. The fit residuals are shown in black. The fitted damping lifetime is of 534 s with a sinusoidal frequency of 86.77 mHz.

Seismic event analysis

It is interesting to analyze the behavior of the tiltmeter during and after the excitation from the two seismic events, one of which is shown in Figure 17. The tiltmeter was excited to relatively high amplitude and oscillated coherently through several periods of hysteresis measurements. After excluding the data during the excitation pulses, a damped sinusoidal function was found to fit to the data of the seismic excitation with less than 1% of residuals (also shown in Figure 17), which also includes contributions from possible seismic aftershock. The fit function and parameters are listed in Table V. The decay following the second shock ($t > 9700$ s) showed clear jumps in the residuals, a sign of additional seismic aftershock activity. The decay time of the fit was 534 ± 1 s that with the resonant frequency of 86.83 mHz yields a quality factor of 145.7. The seismic excitation transients could have been extracted from the data stream as suggested in Ref. 20, but having a single instrument, sitting on a rigid but not seismometry-grade stand, it would not have been possible to properly extract signal from the instrument noise level.

TABLE V. Damped sinus fit parameters. The quality factor estimated from the decay is ∼23.

$A \cos(2\pi f (t-t_o)) \exp(-(t-t_o)/\tau)$	Value	Error
A (V)	0.0001134	0.0000002
τ (s)	534.0	0.6
F (Hz)	0.0867710	0.0000003
t_o (Hz)	8666.5	0.004
χ^2	4.3219×10^{-8}	NA
R	0.99875	NA
Residuals (V r.m.s.)	2×10^{-6}	NA

HYSTERESIS DISCUSSION

Hysteresis is the most important source of error in a tiltmeter or tilt accelerometer because it mimics a fake angular acceleration reading, and/or produces a skewed verticality reading. The three measurements of hysteresis at decreasing excitation pulse amplitudes have shown that the hinge's fractional hysteresis decreases with the pulse amplitude, and becomes compatible with zero hysteresis for very small excursions, which would make the instrument an ideal tilt accelerometer. Anelasticity was observed at intermediate amplitude, but no measurable anelasticity was observed at the lowest excitation amplitudes. The residual hysteresis measured is compatible with both the granularity of the knife-edge structure, and the hysteresis contributed by the copper wiring of the LVDTs and actuators. Although very low hysteresis was measured, wireless sensing and actuating, and improved knife-edge structures with no granularity, both suggested and discussed in the conclusions, would be beneficial, especially to mitigate the hysteresis for the larger excursions that may occur during large seismic events.

Effect of the knife-edge granularity to the oscillator potential

A model of the potential energy controlling the tiltmeter arm is shown in Figure 18. For small oscillations a perfect, loss-less knife-edge would generate a quadratic potential, whose steepness is controlled by the height of the beam's center of mass above the hinge. Smaller, random, potential wells are added to simulate the effects of the granularity of the Tungsten Carbide edge. At large oscillation amplitude (L1–L3 in Figure 18) the wells are of little importance, as the arm has sufficient kinetic energy to "fly" over the potential barriers and wells. At high oscillation amplitude, their only effect is to occasionally delay the oscillation at its end point. The oscillator can remain trapped in secondary wells only if their potential barriers are both higher than the average thermal energy KT and high enough to overcome the kicks contributed by high-frequency vibrational perturbations on the instrument's body. Given the large mass of the arm, vibrations in other degrees of freedom can be expected to be quite effective in keeping the arm free from trapped states. To switch from the equilibrium on a set of grains to another, the hinge has to break and re-form van der Waals bonds, which rob energy from the oscillation. One can expect that, at very low oscillation amplitude (L0) the hinge will eventually reside on a single set of grains, relying only on their elasticity to allow the oscillation. In this regime both loss mechanisms are shut down and the quality factor of the instrument may increase. This may be the cause of the disappearance of hysteresis and anelasticity between the second and third measurement.

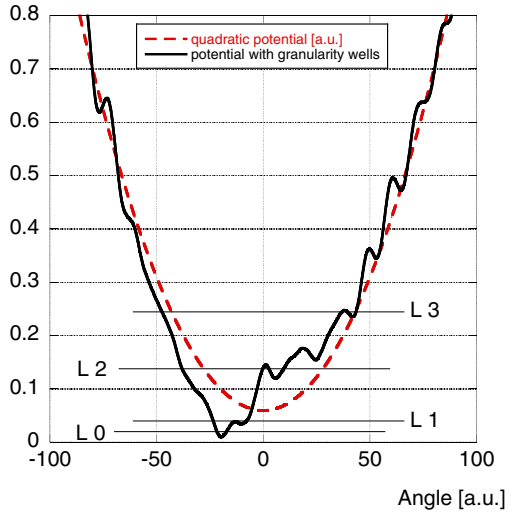

FIG. 18. Model of the potential energy of the tiltmeter: the smooth, dashed curve is the ideal curve with a perfect edge; the bumpy, solid curve includes possible effects from the Tungsten Carbide granularity.

FUTURE IMPROVEMENTS

A number of improvements can be implemented on the prototype design.

Because residual hysteresis is not completely ruled out, even for low excursions, one should mitigate or eliminate the two likely hysteresis sources, i.e., the granularity of the knife edge, and the hysteresis of the electrical wiring.

Granularity free knife-edge

The granularity effect can be mitigated by coating the knife edge with a few μm thick, glassy, hard film, or eliminated altogether by using non-granular materials such as Silicon Carbide. The glassy film, of thickness comparable or larger than the grain size, has the tendency to smooth over the grain edges and provide a more uniform and rounded knife-edge, with lower friction coefficient. The deposited materials can be stronger than Tungsten Carbide (see Tables I and II) and with lower friction coefficient. The radius of curvature would have to be taken into consideration as well; it would add a stability term as discussed in Ref. 29, but it is not expected to change the instrument sensitivity. Coated knife-edges were prepared but could not be tested before the group was disbanded and the laboratory disassembled.

The Silicon Carbide knife-edges may seem ideal because they can be ground with very sharp edges. While no fragility issues were encountered with the Tungsten Carbide wedges and none is expected with coated Tungsten Carbide, an extra sharp, but softer, Silicon Carbide knife-edge may have fragility issues.

Wireless actuation

Wireless controls with sufficiently high authority to run the tiltmeter in feedback mode and sufficiently low noise to preserve its performance may be the toughest challenge. Eddy current dissipation was found to be a nuisance in our prototype, but it could be turned into an advantage by using it as a low noise, wireless actuator. For this the beam end masses would be made of OHFC copper to increase the eddy current repulsion forces. Four identical coils mounted as in Figure 19, with the top right and the bottom left wired in series and the

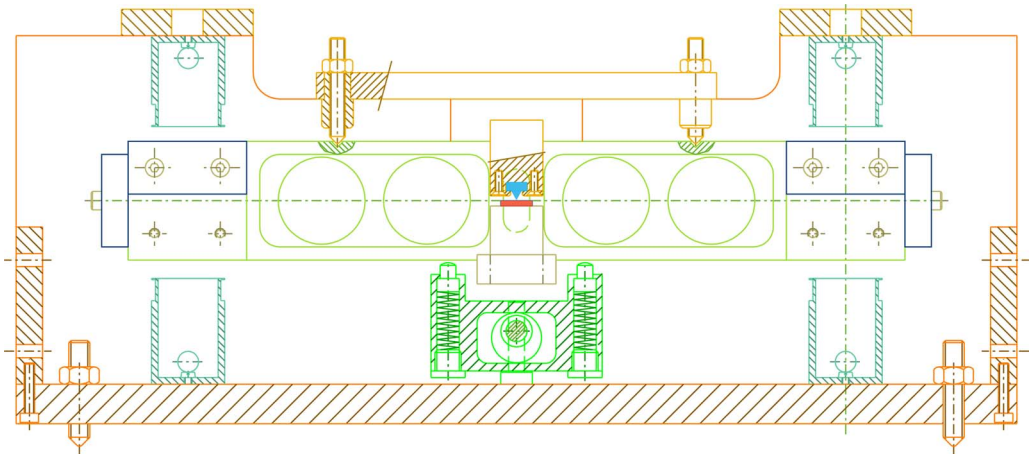

FIG. 19. Schematic of a tiltmeter with a wireless, eddy current actuator.

bottom right in series with the top left would provide the required torque. The two circuits would be driven with the same radiofrequency, changing the overall amplitude to change the authority, and the balance to generate the desired torque.

Fine frequency tuning

When the arm is tuned at 50 mHz the center of mass of the 2.4 kg arm is just 1.2×10^{-4} m below the hinge, providing a 28.8 g m restoring torque. To bring the resonant frequency all the way to zero one needs to add a 2.88 g mass 1 cm above the hinge axis. This level of tuning can be easily achieved with a simple vertical threaded rod and 2 nuts.

Leveling manipulator

A semi-fine leveling can be obtained using a 0–80 horizontal threaded rod holding two 0.12 g nuts. A rotation of one turn of the nuts (∼0.125 mm pitch) yields a torque change of $\sim 30 \times 10^{-9}$ kg m. At 50 mHz tuning it would allow a 10 μradian step. At lower frequency, finer leveling would have to be applied with a mechanical manipulator moving a light cavalier over a horizontal rod, in the fashion used in ancient precision scales, or dynamically, using a fixed bias on the actuators.

CONCLUSIONS

A tiltmeter based on a ceramic knife-edge hinge was built and characterized. Its design parameters and philosophy have been described. The instrument appears to be free of hysteresis for small excursions, which would make it free of the 1/f mechanical noise observed with metallic flexures. The main difficulties encountered were in the low noise actuation for instrument feedback operation. A sensitivity of 5.7×10^{-9} radian/$\sqrt{\text{Hz}}$ at 10 mHz and 6.4×10^{-10} radian/$\sqrt{\text{Hz}}$ at 0.1 Hz were measured in a separate paper.[16] Several ways of improvement for even better instrument performance have been proposed.

ACKNOWLEDGMENTS

The authors gladly acknowledge Carlo Galli for advice on construction techniques and material choice, Gianni Gennaro for help in the instrument design, Charles Hagedorn and Kryshna Venkateswara for many useful discussions. This work has been done by members or visitors of LIGO laboratory in California Institute of Technology, while supported by funding from United States National Science Foundation and operates under cooperative Agreement No. PHY-0757058.

[1] B. Lantz, R. Schofield, B. O'Reilly, D. E. Clark, and D. DeBra, "Review: Requirements for a ground rotation sensor to improve advanced LIGO," Bull. Seismol. Soc. Am. **99**, 980–989 (2009).
[2] Several articles in Bull. Seismol. Soc. Am. **99** (2009).
[3] As presented by Vincent Lhuillier at the LSC-Virgo Meeting, March 2013, SEI Status page 17, internal LIGO document G1300235, see https://dcc.ligo.org/LIGO-G1300235-v2.
[4] A. J. Mullavey *et al.*, "Arm-length stabilisation for interferometric gravitational-wave detectors using frequency-doubled auxiliary lasers," Opt. Exp. **20**(1), 81–89 (2012).
[5] K. Izumi *et al.*, "Multi-color cavity metrology," JOSA A **29**(10), 2092–2103 (2012).
[6] A. Giazotto, "Tilt meter as a tilt-independent accelerometer," Phys. Lett. A **376**, 667–670 (2012).
[7] R. DeSalvo *et al.*, "The role of self-organized criticality in elasticity of metallic springs: Observations of a new dissipation regime," Eur. Phys. J. Plus **126**, 75 (2011).
[8] P. Bak *et al.*, Phys. Rev. Lett. **59**, 381 (1987).
[9] C. Tang and P. Bak, Phys. Rev. Lett. **60**, 2347 (1988).
[10] C. C. Speake *et al.*, "The design and application of a novel high-frequency tiltmeter," Rev. Sci. Instrum. **61**(5), 1500–15003 (1990).
[11] A. N. Luiten *et al.*, "Ground tilt seismic spectrum measured with a new high sensitivity rotational accelerometer," Rev. Sci. Instrum. **68**(4), 1889–1893 (1997).
[12] Y. Cheng *et al.*, "Tilt sensor and servo control system for gravitational wave detection," Class. Quantum Grav. **19**, 1723 (2002).
[13] K. Venkateswara *et al.*, "A high-precision mechanical absolute-rotation sensor," Rev. Sci. Instrum. **85**, 015005 (2014).
[14] D. Rozelle, The hemispherical resonator gyro: From wineglass to the planets, see www.northropgrumman.com/Capabilities/HRG/Documents/hrg.pdf.
[15] Produced by Medicon, 31 Mendeleyev Str., Miass, Chelyabinsk Region, 456320, Russia.
[16] V. Dergachev *et al.*, "A high precision, compact electromechanical ground rotation sensor," Rev. Sci. Instrum. **85**, 054502 (2014).
[17] A. O'Toole, A. Bhawal, M. Asadoor, and R. DeSalvo, Tiltmeter characterization, LIGO-T1000340-v1, see https://dcc.ligo.org/LIGO-T1000340/public.

[18]See http://www.lafer.eu/lafer/index_en.php for properties of Lafer coatings.
[19]H. Tariq *et al.*, "The linear variable differential transformer (LVDT) position sensor for gravitational wave interferometer low-frequency controls," Nucl. Instrum. Meth. Phys. Res. A **489**, 570–576 (2002).
[20]M. Zumberge, J. Berger, J. Otero, and E. Wielandt, "An optical seismometer without force feedback," Bull. Seismol. Soc. Am. **100**(2), 598–605 (2010).
[21]F. Erasmo Peña Arellano, H. Panjwani, L. Carbone, and C. C. Speake, "Interferometric measurement of angular motion," Rev. Sci. Instrum. **84**, 043101 (2013).
[22]F. E. Peña Arellano, Interferometer readout for tiltmeter, see https://dcc.ligo.org/LIGO-P1300166/public.
[23]V. Greco, C. Iemmi, S. Ledesma, G. Molesini, and F. Quercioli, "Multiphase homodyne interferometry: Analysis of some error sources," Appl. Opt. **34**(13), 2207 (1995).
[24]W. Zeller, L. Naehle, P. Fuchs, F. Gerschuetz, L. Hildebrandt, and J. Koeth, "DFB lasers between 760 nm and 16 mm for sensing applications," Sensors **10**(4), 2492–2510 (2010).
[25]L. V. T. Nguyen, "Distributed-feedback (DFB) laser coherence and linewidth broadening," Technical Report No. DSTO-RR-0263, DSTO, September, 2003.
[26]See the single-frequency laser SFL1550P in www.thorlabs.com.
[27]M. J. Usher *et al.*, "An instrument for discriminating between acceleration and ground tilt in horizontal component seismometers," Meas. Sci. Technol. **3**, 574–577 (1992).
[28]M. Mantovani *et al.*, "One hertz seismic attenuation for low frequency gravitational waves interferometers," Nucl. Instrum. Meth. Phys. Res. A **554**, 546–554 (2005).
[29]E. Cesarini *et al.*, "A "gentle" nodal suspension for measurements of the acoustic attenuation in materials," Rev. Sci. Instrum. **80**, 053904 (2009).